Iterated Fourier Transform Systems: A Method for Frequency Extrapolation

Gregory S. Mayer and Edward R. Vrscay

Department of Applied Mathematics
Faculty of Mathematics
University of Waterloo
Waterloo, Ontario, Canada N2L 3G1
gsmayer@uwaterloo.ca, ervrscay@uwaterloo.ca

1 Introduction

In this paper we introduce a fractal-based method over (complex-valued) Fourier transforms of functions with compact support $X \subset \Re$. This method of "iterated Fourier transform systems" (IFTS) has a natural mathematical connection with the fractal-based method of "iterated function systems with greyscale maps" (IFSM) in the spatial domain [6,7]. A major motivation for our formulation is the problem of resolution enhancement of band-limited magnetic resonance images. In an attempt to minimize sampling/transform artifacts, it is our desire to work directly with the raw frequency data provided by an MR imager as much as possible before "returning" to the spatial domain. In this paper, we show that our fractal-based IFTS method can be tailored to perform frequency extrapolation.

2 MRI and the Frequency Extrapolation Problem

Here, we briefly outline the problem of frequency extrapolation, with particular focus on an important source of such problems: magnetic resonance imaging (MRI), where the raw data is a Fourier spectrum of the desired image. For simplicity of notation and presentation, we consider only one-dimensional MRI procedures in this paper. We shall assume that the object of concern is located within an interval $X = [-x_{max}, x_{max}]$ on the x-axis. It is the *proton density* of the object, to be denoted as $\rho(x)$ for $x \in X$, to which the magnetic resonance scanner responds. The (spatially) linearly varying magnetic field in the magnetic resonance spectrometer produces a complex-valued signal $s(k)$ of the real-valued frequency parameter k. The relation between $s(k)$ and the proton density function $\rho(x)$ may be expressed as follows [10,13,9]:

$$s(k) = \int_{-\infty}^{+\infty} \rho(x) \exp(-i2\pi kx) dx, \qquad k \in \Re. \tag{1}$$

In other words, $s(k)$ is related to $\rho(x)$ via the Fourier transform [3].

M. Kamel and A. Campilho (Eds.): ICIAR 2007, LNCS 4633, pp. 728–739, 2007.

In practice, however, the true proton density, $\rho(x)$, cannot be obtained, but rather must be estimated. Since the object being imaged has a finite size, its Fourier spectrum necessarily has infinite support. But the data can only be collected over a finite interval: Without loss of generality, we shall assume that the k-space data is acquired over an interval of finite size and centered over the origin: $k \in K = [-k_{max}, k_{max}]$. Another consideration is that the k-space data must also be sampled. Ultimately, post-processing and reconstruction can yield only discrete approximations to $\rho(x)$, with finite spatial resolution, Δx.

Increasing the spatial resolution in MRI has often been performed by optimizing the capabilities of the imaging hardware. However, any improvement in the resolving power of MRI would further increase the efficacy of this modality.

The following simple expression,

$$\Delta x = \frac{1}{2k_{max}}, \tag{2}$$

naturally demonstrates the fundamental relationship between the spectral extent, $2k_{max}$, and the capacity of the image to represent features of the object over different spatial scales. Enhancing the spatial resolution via any chosen post-processing strategy involves the estimation of frequencies beyond the maximum measured frequency, k_{max}.

Early investigations on frequency domain extrapolation include the famous work by Slepian and Pollack [17] that employed prolate spheroidal wave functions, and the well known Papoulis-Gerchberg algorithm [8,16]. An enormous amount of literature on frequency domain extrapolation followed, e.g., [18,11]. (In no way are our references intended to be complete.) Later, frequency extrapolation was considered in the field of MRI (for example, see [12,13,15]).

3 Iterated Function Systems with Greyscale Maps (IFSM)

In this section we outline the basic ideas of a special class of *iterated function systems with greyscale maps* (IFSM), a fractal-based method over functions. The treatment is brief and quite specific to our applications – for more generality and details, the reader is referred to [6,7].

In what follows, (X, d) denotes a compact metric *base space*, the spatial support of our signal or image. Here, our primary applications will be one-dimensional signals. Therefore, unless otherwise indicated, we shall let $X = [-1, 1]$. We also let $\mathcal{B}(X)$ denote a suitable Banach space of functions $u : X \to \Re$. In applications, these functions will be bounded, in which case we may also wish to specify their range R_g, i.e., $u : X \to R_g$, where $R_g \subseteq \Re$. (In the practical case of image processing, for example, we may wish R_g to be $[0, 1]$.)

An N-map *affine IFSM* is defined by the following:

1. **The spatial IFS component: $\mathbf{w} = \{w_1, \cdots, w_N\}$**, a set of affine contraction maps $w_k : X \to X$ having the form

$$w_k(x) = s_k x + a_k, \quad |s_k| < 1, \quad k = 1, 2, \cdots, N. \tag{3}$$

We shall denote $X_k = w_k(X) = \{w_k(x) \mid x \in X\}$.

2. **The greyscale component:** $\mathbf{\Phi} = \{\phi_1, \cdots, \phi_N\}$, a set of associated affine greyscale maps $\phi_k : R_g \to R_g$ having the form

$$\phi_k(t) = \alpha_k t + \beta_k, \quad k = 1, 2, \cdots, N. \tag{4}$$

Associated with the above N-map affine IFSM is the *fractal transform* operator $\hat{T} : \mathcal{B}(X) \to \mathcal{B}(X)$. Given a function $u \in \mathcal{B}(X)$, its image $v = Tu$ will be defined as

$$(\hat{T}u)(x) = \sum_{k=1}^{N} f_k(x) = \sum_{k=1}^{N} \left[\alpha_k u(w_k^{-1}(x)) + \beta_k\right] I_{X_k}(x). \tag{5}$$

Here $I_A(x)$ denotes the *indicator* or *characteristic function* of a set $A \subseteq X$: $I_A(x) = 1$ if $x \in A$ and $I_A(x) = 0$ otherwise. Each *fractal component* f_k is supported on the subset X_k.

Geometrically, the action of the fractal transform $\hat{T}$ may be viewed in terms of its action on the graph of u which is supported on X. Each term $u(w_k^{-1}(x))$ represents a spatially-contracted copy of the graph of u which is supported on the subset $X_k = w_k(X)$. The greyscale map ϕ_i then distorts this copy in the greyscale direction R_g to produce the fractal component $f_i(x)$. The fractal transform $\hat{T}$ then adds up these fractal components to produce $(\hat{T}u)(x)$.

We now consider the $\mathcal{L}^p$ function spaces, i.e., $\mathcal{B}(X) = \mathcal{L}^p(X)$, $p = 1, 2, \cdots$, where

$$\mathcal{L}^p(X) = \left\{ u : X \to \mathbf{R} \mid \| u \|_p = \left[\int_X |u(x)|^p \right]^{1/p} dx \; < \; \infty \right\}.$$

Consider a fixed integer $p \geq 1$. Then for any $u, v \in \mathcal{B}(X)$ [6],

$$\| Tu - Tv \|_p \;\; \leq \;\; C_p \, \| u - v \|_p, \quad C_p = \sum_{k=1}^{N} |s_k|^{1/p} |\alpha_k|. \tag{6}$$

If $C_p < 1$ then $\hat{T}$ is a contraction over the space $\mathcal{L}^p(X)$. From Banach's Fixed Point Theorem, there exists a unique fixed point function $\bar{u} \in \mathcal{L}^p(X)$ such that $\bar{u} = T\bar{u}$. Moreover, consider any "seed" function $u_0 \in \mathcal{L}^p(X)$. If we construct the sequence of functions $u_n \in \mathcal{L}^p(X)$ according to the iteration scheme

$$u_{n+1} = Tu_n, \quad n = 0, 1, 2, \cdots, \tag{7}$$

then the sequence u_n converges to $\bar{u}$, i.e., $\lim_{n\to\infty} \| u_n - \bar{u} \|_p = 0$.

From Eq. (5), the relation $\bar{u} = \hat{T}\bar{u}$ implies that the fixed point $\bar{u}$ exhibits *self-similarity*, i.e., it may be expressed as a sum of spatially-contracted and greyscale-modified copies of itself.

3.1 Inverse Problem of Approximation Using Contraction Maps

One of the original motivations for studying fractal-based methods was fractal image compression [4,2,14]. The underlying mathematical principle, which we outline briefly, is that of approximation by fixed points of contractive mappings.

Let (Y, d_y) be a complete metric space and $Con(Y)$ be a family of contraction mappings on Y. Given a "target" element $y \in Y$, find a contraction mapping $\hat{T}$ with fixed point $\bar{y}$ such that $\bar{y}$ approximates y as closely as possible, i.e., the distance $d_Y(y, \bar{y})$ is as small as possible.

Instead of storing the image y, one stores the parameters that define $\hat{T}$. The approximation $\hat{y}$ may then be generated by the iteration procedure in Eq. (7).

Such *inverse problems* involving fractal transforms are generally intractable. Most, if not all, fractal coding methods rely on the following result, a consequence of Banach's Fixed Point Theorem:

Let $\hat{T} : Y \to Y$ be a contraction mapping with factor $c_T \in [0, 1)$. Let $\bar{y}$ be the fixed point of $\hat{T}$. Then for all $y \in Y$,

$$d_Y(y, \bar{y}) \leq \frac{1}{1 - c_T} d_Y(y, Ty). \tag{8}$$

In the fractal coding literature, this result is known as the *Collage Theorem* [1]. Instead of searching for contraction maps $\hat{T}$ that minimize the approximation error $d_Y(y, \bar{y})$, one tries to minimize the so-called *collage distance* $d_Y(y, Ty)$ (while keeping a control on the contractivity factor c_T). In other words, one searches for maps $\hat{T}$ that send the target y as close as possible to itself. This procedure is often called *collage coding*.

In applications, one normally fixes the affine contraction maps w_i and determine the optimal greyscale maps ϕ_i. In principle, the minimization of the squared $\mathcal{L}^2$ collage distance is a quadratic programming problem in the greyscale parameters α_k and β_k, subject to constraints that guarantee contractivity of the fractal transform $\hat{T}$. For further discussion, readers may wish to consult [4,2,14].

4 From Fractal Transforms to IFTS

Our goal is now to formulate an IFS-type method over Fourier transforms. Given a function $u \in \mathcal{B}(X)$, consider its complex-valued Fourier transform $U = \mathcal{F}[u]$, defined as follows,

$$U(\omega) = \int_{-\infty}^{\infty} e^{-i\omega x} u(x)\, dx, \quad \omega \in \Re. \tag{9}$$

Note that we shall work with the angular frequency $\omega = 2\pi k$ for simplicity of notation. Now suppose that $v = \hat{T}u$, where $\hat{T}$ is the fractal transform in Eq. (5). Let the Fourier transform of v be denoted by

$$\mathcal{F}[v] = V(\omega) = \int_{-\infty}^{\infty} e^{-i\omega x} v(x)\, dx. \tag{10}$$

We now derive the relationship between the Fourier transforms U and V.

First, substitute Eq. (5) into Eq. (10) to give

$$V(\omega) = \sum_{k=1}^{N} \alpha_k \int_{-\infty}^{\infty} e^{-i\omega x} u(w_k^{-1}(x))\, dx + \sum_{k=1}^{N} \beta_k \int_{-\infty}^{\infty} e^{-i\omega x} I_{X_k}(x)\, dx. \quad (11)$$

In the first set of integrals, we make the change of variable $y = w_k^{-1}(x)$, implying that $x = w_k(y) = s_k y + a_k$ and $dx = s_k\, dy$. These integrals then become

$$\begin{aligned} \int_{-\infty}^{\infty} e^{-i\omega x} u(w_k^{-1}(x))\, dx &= s_k \int_X e^{-i\omega(s_k y + a_k)} u(y)\, dy \\ &= s_k e^{-ia_k\omega} \int_{-\infty}^{\infty} e^{-is_k\omega y} u(y)\, dy \\ &= s_k e^{-ia_k\omega} U(s_k\omega). \end{aligned} \quad (12)$$

(Recall that u vanishes outside the interval X.) In a similar way,

$$\begin{aligned} \int_{-\infty}^{\infty} e^{-i\omega x} I_{X_k}(x)\, dx &= s_k e^{-ia_k\omega} \int_{-\infty}^{\infty} e^{-is_k\omega x} I_X(x)\, dx \\ &= s_k e^{-ia_k\omega} F_X(s_k\omega), \end{aligned} \quad (13)$$

where

$$F_X(w) = \int_X e^{-i\omega x}\, dx. \quad (14)$$

Substitution of these two sets of results into Eq. (11) yields the final result

$$V(\omega) = (\hat{M}U)(\omega) = \sum_{k=1}^{N} \left[\alpha_k s_k e^{-ia_k\omega} U(s_k\omega) \;+\; \beta_k s_k e^{-ia_k\omega} F_X(s_k\omega)\right]. \quad (15)$$

Eq. (15) defines the action of the operator $\hat{M}$ that is induced by the fractal transform $\hat{T}$. The relation $v = \hat{T}u$ implies that $V = \hat{M}U$, where $U = \mathcal{F}[u]$ and $V = \mathcal{F}[v]$. Technically, $\hat{M}$ is a mapping from the space of functions that are Fourier transforms of functions in $\mathcal{B}(X)$ to itself – let us call this space $\mathcal{B}^{FT}(X)$. We shall refer to $\hat{M}$ as an IFTS operator, for *iterated function systems on Fourier transforms*.

Let us compare the frequency-space result in Eq. (15) with its spatial counterpart in Eq. (5). Here, $V(\omega)$ is a sum of distorted, *frequency-expanded* copies of $U(\omega)$ along with various modified copies of sinc functions. Note that the value of $U(\omega)$ is determined by values of U at lower frequencies $s_k\omega$. This will provide the mechanism for frequency extrapolation.

Because of space limitations, we state some results without proofs.

1. The space $\mathcal{B}^{FT}(X)$ is closed. Furthermore $\hat{M}$ maps $\mathcal{B}^{FT}(X)$ to itself.
2. Let $U, V \in \mathcal{B}^{FT}(X)$. Then using the $\mathcal{L}^p$ norm (assuming that the integrals exist),
$$\| \hat{M}U - \hat{M}V \|_p \;\leq\; C_p \| U - V \|_p, \quad (16)$$
where C_p is given in Eq. (6). In other words, the IFSM operator $\hat{T}$ and the IFTS operator $\hat{M}$ have the same Lipschitz constant.

3. In the case that $C_p < 1$, then both $\hat{T}$ and $\hat{M}$ are contractive over their respective metric spaces. Their respective fixed points, $\bar{u} \in \mathcal{B}(X)$ and $\bar{U} \in \mathcal{B}^{FT}(X)$, will be related as $\bar{U} = \mathcal{F}[\bar{u}]$.

Examples

1. The following $N = 2$-map affine IFSM on $X = [-1, 1]$:

$$w_1(x) = \frac{1}{2}x - \frac{1}{2},\ \phi_1(t) = \frac{1}{2}t + \frac{1}{2}, \quad w_2(x) = \frac{1}{2}x + \frac{1}{2},\ \phi_2(t) = \frac{1}{2}t + \frac{1}{2}. \tag{17}$$

   Note that $X_1 = w_1(X) = [-1, 0]$ and $X_2 = w_2(X) = [0, 1]$: The two sets are nonoverlapping in the $\mathcal{L}^2$ sense, even though they "touch" at $x = 0$. The fixed point for the associated IFSM operator $\hat{T}$, cf. Eq. (5), is $\bar{u}(x) = 1$ for $x \in X$. The fixed point for the corresponding IFTS operator $\hat{M}$, cf . Eq. (15) is the real-valued function $\bar{U}(\omega) = 2\dfrac{\sin\omega}{\omega} = \mathcal{F}(\bar{u})$.
2. A perturbation of the above system:

$$w_1(x) = \frac{3}{5}x - \frac{2}{5},\ \phi_1(t) = \frac{3}{10}t + \frac{1}{2}, \quad w_2(x) = \frac{3}{5}x + \frac{2}{5},\ \phi_2(t) = \frac{1}{2}t + \frac{1}{2}. \tag{18}$$

   Here $X_1 = w_1(X) = [-1, \frac{2}{5}]$ and $X_2 = w_2(X) = [-\frac{2}{5}, 1]$: The two sets overlap over the interval $[-\frac{2}{5}, \frac{2}{5}]$. The fixed points, $\bar{u}$ and $\bar{U}$ for, respectively, the IFSM operator $\hat{T}$ and the IFTS operator $\hat{U}$ are shown in Figure 1 below. Note that the attractor $\bar{u}$ possesses a self-similarity – the "piling up" of function values over the overlap region is repeated over the entire interval X under the action of the IFS maps w_i. On the other hand, the Fourier transform $\bar{U}$ is a mild perturbation of the transform of Example 1, most notably in the non-zero imaginary part. The attractors were computed by means of iteration of the operators, $\hat{T}$ and $\hat{U}$ in their respective spatial and frequency domains.

5 Inverse Problem of IFTS and Frequency Extrapolation

We now have the ingredients to perform the following inverse problem of Fourier transform approximation: Given a "target" Fourier transform $U \in \mathcal{B}^{FT}(X)$, find an IFTS operator $\hat{M}$ with fixed point $\bar{U}$ that approximates U to an acceptable accuracy.

We adopt a *collage coding* strategy, cf. Eq. (8), and look for an operator $\hat{M}$ that minimizes the collage distance $\Delta = d_{FT}(U, \hat{M}U)$, where d_{FT} denotes a suitable metric on the space of functions $\mathcal{B}^{FT}(X)$.

5.1 Solving the IFTS Inverse Problem

Our procedure will mimic the usual procedure of IFSM fractal coding: We shall fix N, the number of components in the IFTS operator $\hat{M}$ in Eq. (15), as well

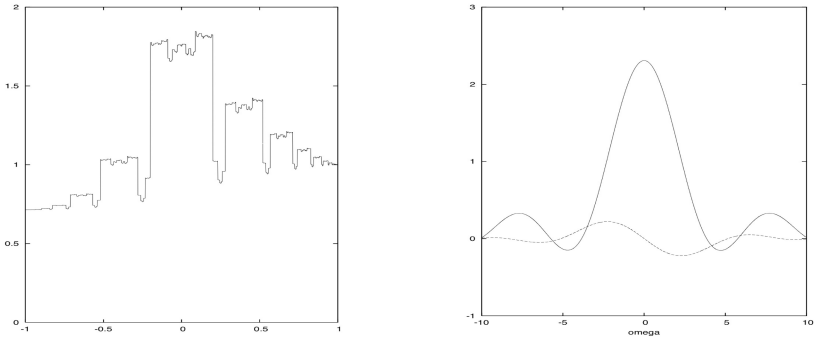

(a) IFSM fixed point $\bar{u}$ (b) IFTS fixed point $\bar{U}$

Fig. 1. Fixed point attractors (a) $\bar{u}$ and (b) $\bar{U}$ (real and imaginary parts) for the IFSM/IFTS of Example 2 in text

as the affine spatial contraction maps w_i in Eq. (3), $1 \leq k \leq N$. The optimal values of the real greyscale coefficients α_i and β_i in Eq. (4) will then be given by

$$(\alpha^*, \beta^*) \;=\; \arg \min_{(\alpha,\beta)\in \Pi} d_{FT}(U, \hat{M}(\mathbf{s}, \mathbf{a}, \alpha, \beta)U). \tag{19}$$

Here, $\Pi \in \Re^{2N}$ denotes a *feasible parameter space* that ensures contractivity of the IFTS operator $\hat{M}$.

As in traditional fractal image coding, it is convenient to use the $\mathcal{L}^2$ metric. The squared $\mathcal{L}^2$ collage distance is

$$\begin{aligned} \Delta^2(\alpha, \beta) &= \| \, U - \hat{M}U \, \|_2^2 \\ &= \int_{\Re} |U(\omega) - \sum_{k=1}^{N} s_k \alpha_k e^{-ia_k\omega} U(s_k\omega) \\ &\qquad - \sum_{k=1}^{N} s_k \beta_k e^{-ia_k\omega} F_X(s_k\omega)|^2 \, d\omega. \end{aligned} \tag{20}$$

Note that Δ^2 may also be rewritten as a quadratic form,

$$\Delta^2(\mathbf{x}) = \| \, U \, \|^2 + \mathbf{x}^T \mathbf{A}\mathbf{x} + \mathbf{b}\mathbf{x}, \tag{21}$$

where $\mathbf{x}^T = (\alpha_1, \cdots, \alpha_N, \beta_1, \cdots, \beta_N)$. Here, $\mathbf{A}$ may be expressed as a $2N \times 2N$ symmetric real matrix and $\mathbf{b}$ a real $2N$-vector. The minimization of Δ^2 may now be accomplished with quadratic programming algorithms, generally at a fraction of the time required for gradient descent methods.

Of course, the minimization must be performed with constraints. The contractivity constraint $C_2 < 1$ from Eq. (6) is a very strict condition, having been obtained by a simple application of the triangle inequality. From a knowledge of the maps w_i involved and the overlapping/nonoverlapping properties of the

associated sets X_i, one may be able impose more relaxed conditions. Additional constraints may be imposed from the requirement that the associated spatial fixed point function $\bar{u}(x)$ be nonnegative over X, e.g., $\alpha_k, \beta_k \geq 0$.

Another concern is to make the collage distance "suitably small." *Theoretically* – and we emphasize this word – the collage distance can be made arbitrarily small by suitably increasing the refinement of the partition produced by the spatial IFS maps over the interval X. (The "proof" is basically the same as presented in [7].) A systematic and quite effective refinement is produced by using N-map truncations $\mathbf{w}_N$ of the infinite set $\mathbf{w} = \{w_{11}, w_{12}, w_{21}, \cdots, \}$ of spatial IFS maps on $X = [-1, 1]$ given by

$$w_{nj} = \frac{1}{2^n}(x + 2j - 1 - 2^n), \quad n = 1, 2, \cdots, \quad 1 \leq j \leq 2^n. \tag{22}$$

This system of maps produces a decomposition of X into dyadic subintervals. The natural choices for N are $2, 2{+}4 = 6, 2{+}4{+}8 = 14$, ..., $2{+}\cdots{+}2^p = 2^{p+1}{-}2$, $p = 1, 2, \cdots$, which produce complete dyadic refinements of $[-1, 1]$ down to $\Delta x = 2^{-(p-1)}$. This system also permits "mixing" between overlapping intervals of varying size. Such a strategy was adopted successfully in [5].

Example 3: We consider a complex-valued Fourier transform $U(\omega)$, defined over the interval $\Omega = [-100, 100]$, the real and imaginary components of which are plotted in Figures 2(a) and 2(b), respectively (solid line plot). Its inverse Fourier transform, the spatial function $u(x)$, is plotted in Figure 3(a) (apart from ringing artifacts outside the interval $X = [-1, 1]$ due to the finiteness of Ω).

With $U(\omega)$ as our target function, we applied $\mathcal{L}^2$ collage coding, using the system of "dyadic" IFS maps given in Eq. (22). For $N = 2, 6$ and 14, the minimal collage errors Δ obtained were 2.13, 1.70 and 1.08, respectively. The Harwell HSL Archive FORTRAN subroutine VE17AD was used to solve the associated quadratic programming problems. In all cases, the solution was provided in a

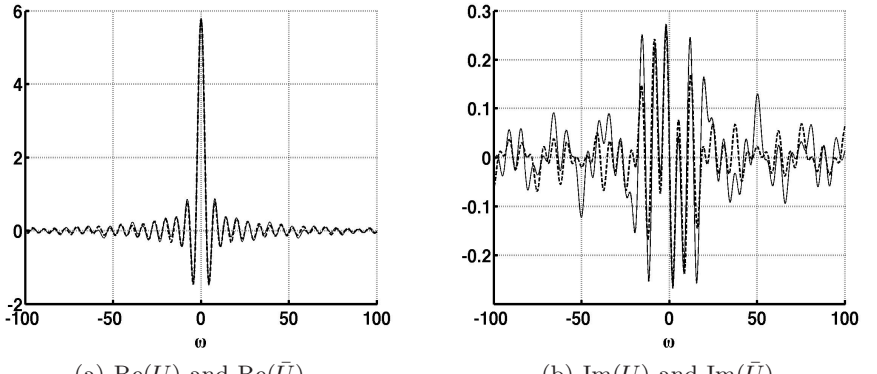

(a) Re(U) and Re($\bar{U}$) (b) Im(U) and Im($\bar{U}$)

Fig. 2. Target $U(\omega)$ (solid plot) and fixed point approximation $\bar{U}(\omega)$ (dotted plot) yielded by a 14-IFS map IFTS

fraction of a second. (In contrast, gradient search methods required on the order of an hour of computer time to solve the 14-map problem.) In Figures 2(a) and 2(b) we have plotted the real and imaginary components of the fixed point $\bar{U}(\omega)$ of the 14-map IFTS. Note that the relatively well-behaved real part of the target $U(\omega)$ is very well approximated over the interval Ω.

5.2 Frequency Extrapolation

In practical applications, e.g., magnetic resonance imaging, the target Fourier transform U in our inverse problem formulation is known only over a finite interval, say, $\Omega_0 = [-\omega_0, \omega_0]$. We shall denote this truncated, bandlimited transform as U_0. Our motivation to solve the inverse problem is to use U_0 to estimate higher frequency components of U, thereby achieving higher resolution in the spatial domain.

The use of IFTS to perform frequency extrapolation is motivated by the action of the IFTS operator $\hat{M}$ in Eq. (15) and noted earlier: The value of $V(\omega) = (\hat{M}U)(\omega)$ is determined by values of U at lower frequencies $s_k\omega$. Consider any U_0 with support $\Omega_0 = [-\omega_0, \omega_0]$. Now let $U_1 = \hat{M}U_0$. It follows that the support of U_1 is the interval $\Omega_1 = [-A\omega_0, A\omega_0]$, where $A = [\max_k |s_k|]^{-1}$. In general, the support of $U_n = \hat{M}^n U_0$ is $\Omega_n = [-A^n\omega_0, A^n\omega_n]$. In this way, lower frequency information makes its way outward, implying frequency extrapolation.

Working with the truncated transform U_0, however, introduces an additional approximation error into the *collage coding* procedure. The following result is a straightforward consequence of the Collage Theorem and the triangle inequality:

> Given a target transform $U \in \mathcal{B}^{FT}(X)$ and an approximation U_0 to U, with $d_{FT}(U, U_0) = \delta$. Now suppose that we perform collage coding on U_0, that is, we find an N-map affine IFTS $\hat{M}_0$ with contraction factor $c_0 \in [0, 1)$ such that $d_{FT}(U_0, \hat{M}_0 U_0) \leq \epsilon$, where $\epsilon > 0$. Then
>
> $$d_{FT}(U, \bar{U}_0) \leq \frac{1}{1 - c_0}\epsilon + \delta, \tag{23}$$
>
> where $\bar{U}_0$ is the fixed point of M_0.

Of course, in the limit $\delta \to 0$, we retrieve the Collage Theorem, cf. Eq. (8).

No matter how small we may force the collage error ϵ by suitable refinement, the error $\delta > 0$ serves as a barrier toward the approximation of our (unknown) target U with the fixed point $\bar{U}$, as will be seen below.

Example 3 revisited: Let us return to the target transform $U(\omega)$ presented in Figure 2, with support $[-100, 100]$. When inverted, it yields the spatial profile $u(x)$ in Figure 3(a). Now suppose that we are given only one-half of this data, i.e. $U_0 = U|_{[-50,50]}$, with support $\Omega_0 = [-50, 50]$. Inversion of U_0 yields the lower-resolution profile $u_0(x)$ pictured in Figure 3(b). The $\mathcal{L}^2$ error of approximation is $\delta = \| u - u_0 \|_2 = 0.066$. In this example, all spatial functions on $[-1, 1]$ have been normalized in the $\mathcal{L}^2$ norm.

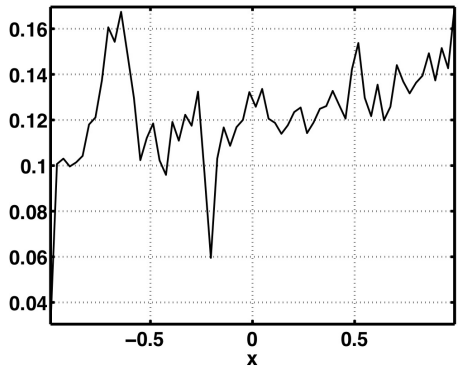

(a) Target function $u = \mathcal{F}^{-1}(U)$

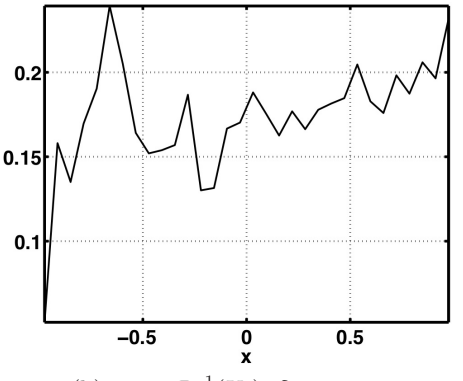

(b) $u_0 = \mathcal{F}^{-1}(U_0)$, $\delta = 0.066$

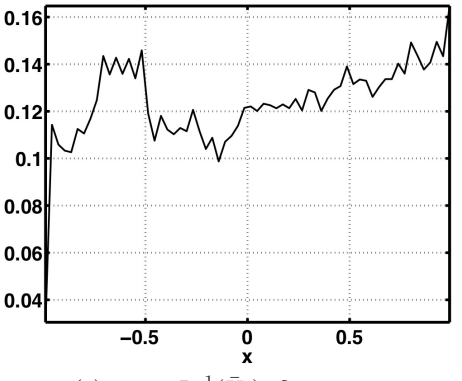

(c) $\bar{u}_0 = \mathcal{F}^{-1}(\bar{U}_0)$, $\delta = 0.100$

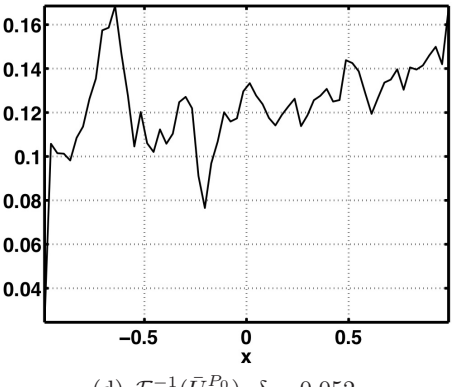

(d) $\mathcal{F}^{-1}(\bar{U}_0^{P_0})$, $\delta = 0.052$

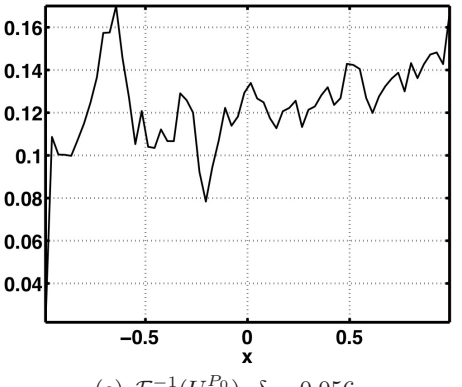

(e) $\mathcal{F}^{-1}(U_1^{P_0})$, $\delta = 0.056$

Fig. 3. (a): The target spatial function $u(x) = \mathcal{F}^{-1}(U)$ corresponding to the Fourier transform U plotted in Fig. 2. (b)-(e): Approximations yielded by the bandlimited data U_0 and various frequency extrapolation methods applied to U_0, as described in text. $\mathcal{L}^2$ approximation errors are also given. All functions have been normalized in $\mathcal{L}^2$ on $X = [-1, 1]$.

Collage coding of U_0 with a 14-map IFTS, using the w_{ij} maps in Eq. (22), produces a fixed point $\bar{U}_0$, the inversion of which is shown in Fig. 3(c). Even though $\bar{u}_0$ has much more spatial resolution, it is a poorer approximation to u than u_0, with an $\mathcal{L}^2$ error $\delta = 0.100$. One possible reason for this observation: It is not guaranteed that the given low frequency component of U – namely, U_0 – is well approximated by $\bar{U}_0$. In order to bypass this problem – and in the spirit of the Papoulis-Gerchberg algorithm for frequency extrapolation – we simply replace the frequency components $\bar{U}_0|_{\Omega_0}$ with the original data U_0, i.e.,

$$\bar{U}_0^{P_0}(\omega) = [1 - I_{\Omega_0}(\omega)]\bar{U}_0(\omega) + U_0(\omega), \qquad \omega \in \Omega. \tag{24}$$

Mathematically, $\bar{U}_0^{P_0}$ is the projection of $\bar{U}_0$ onto the subspace P_0 of transforms with frequency subspectrum U_0 on Ω_0.

Inversion of $\bar{U}_0^{P_0}$ over $[-100, 100]$ yields the spatial profile pictured in Fig. 3(d). Visually, it appears to be a much better higher-resolution approximation to u than $\bar{u}_0$. Quantitatively, its $\mathcal{L}^2$ error of $\delta = 0.052$ is also smaller. This $\mathcal{L}^2$ error is also lower that that of u_0, which achieves one of the main goals of this entire exercise.

Another strategy is to consider the fact that collage coding minimizes the distance between a target U and its image $\hat{M}U$. For this reason, we also consider the following construction,

$$U_1^{P_0}(\omega) = [1 - I_{\Omega_0}(\omega)](\hat{M}U_0)(\omega) + U_0(\omega). \tag{25}$$

In other words, we collage code the original data U_0, construct the first iterate $U_1 = \hat{M}_0 U_0$ and once again project onto the subspace P_0. The resulting spatial profile is shown in Fig. 3(e). It also provides a very good higher-resolution approximation to the target spatial profile $u(x)$, both numerically ($\mathcal{L}^2$ approximation error is $\delta = 0.056$) as well as visually.

Our approach in quantifying the relative quality of our reconstructions obtained using different techniques is consistent with what is commonly used in the MRI literature. Measures of error based on the $\mathcal{L}^2$ metric, and "observer measures" are both commonly used strategies to compare results obtained from different post-processing algorithms (see, e.g., [12,15]).

Finally, the above computations represent only a preliminary study of the IFTS method and its possible application to frequency extrapolation. One may also define more general operators that combine contractions along with projections. It is our intention to discuss these aspects elsewhere.

Acknowledgements

This research was supported in part by the Natural Sciences and Engineering Research Council of Canada (NSERC) in the form of a Discovery Grant (ERV) and a Postgraduate Scholarship (GSM), which are hereby gratefully acknowledged.

References

1. Barnsley, M.F., Ervin, V., Hardin, D., Lancaster, J.: Solution of an inverse problem for fractals and other sets. Proc. Nat. Acad. Sci. 83, 1975–1977 (1986)
2. Barnsley, M.F., Hurd, L.P.: Fractal Image Compression. A.K. Peters, Wellesley, MA (1993)
3. Bracewell, R.: The Fourier Transform and its Applications, 2nd edn. McGraw-Hill, New York (1978)
4. Fisher, Y.: Fractal Image Compression. Springer Verlag, New York (1995)
5. Forte, B., Vrscay, E.R.: Solving the inverse problem for measures using iterated function systems: A new approach. Adv. Appl. Prob. 27, 800–820 (1995)
6. Forte, B., Vrscay, E.R.: Theory of generalized fractal transforms. In: Fisher, Y. (ed.) Fractal Image Encoding and Analysis. NATO ASI Series F, vol. 159, Springer, New York (1998)
7. Forte, B., Vrscay, E.R.: Inverse problem methods for generalized fractal transforms, In: Fractal Image Encoding and Analysis, ibid.
8. Gerchberg, R.W.: Super-resolution through Error Energy Reduction. Optica Acta 21(9), 709–720 (1974)
9. Haacke, M.E., Brown, R.W., Thompson, M.R., Venkatesan, R.: Magnetic Resonance Imaging: Physical Principles and Sequence Design. John Wiley & Sons, Inc, USA (1999)
10. Hinshaw, W., Lent, A.: An Introduction to NMR Imaging: From the Bloch Equation to the Imaging Equation. Proceedings of the IEEE 71(3), 338–350 (1983)
11. Jain, A., Ranganath, S.: Extrapolation Algorithms for Discrete Signals with Application in Spectral Estimation. IEEE Trans. ASSP 29(4), 830–845 (1981)
12. Liang, Z., Boada, F.E., Constable, R.R., Haacke, M.E., Lauterbur, P.C., Smith, M.R.: Constrained Reconstruction Methods in MR Imaging. Rev. Mag. Res. Med. 4, 67–185 (1992)
13. Liang, Z., Lauterbur, P.C.: Principles of Magnetic Resonance Imaging, A Signal Processing Perspective. IEEE Press, New York (2000)
14. Lu, N.: Fractal Imaging. Academic Press, New York (1997)
15. McGibney, G., Smith, M.R., Nichols, S.T., Crawley, A.: Quantitative Evaluation of Several Partial Fourier Reconstruction Algorithms Used in MRI. Mag. Res. Med. 30, 51–59 (1993)
16. Papoulis, A.: A New Algorithm in Spectral Analysis and Band-Limited Extrapolation. IEEE Trans. Cir. Sys. 22(9), 735–742 (1975)
17. Slepian, D., Pollack, H.O.: Prolate Spheroidal Wave Functions, Fourier Analysis and Uncertainty - I. Bell System Tech. J., pp. 43-63 (1961)
18. Youla, D.: Generalized Image Restoration by the Method of Alternating Orthogonal Projections. IEEE Trans. Cir. Sys. 25(9) (1978)